AIAA JOURNAL
Vol. 30, No. 3, March 1992

Transient Behavior of Supersonic Flow Through Inlets

H. S. Pordal,* P. K. Khosla,† and S. G. Rubin‡
University of Cincinnati, Cincinnati, Ohio 45221

A solution technique to compute inlet flow behavior is presented. The phenomena of inlet unstart and restart are investigated using a flux-split procedure applied to the Euler and reduced Navier-Stokes (RNS) equations. A time-consistent, direct sparse matrix solver in conjunction with a domain decomposition strategy is applied to compute the transient flow behavior both internal and external to the inlet. Time-varying shocks and time-varying recirculation regions are efficiently analyzed. The code is quite general and is suitable for the computation of flow for a wide variety of geometries and over a wide range of Mach and Reynolds numbers.

Nomenclature

a	= speed of sound
$A, AM, B, C, CM, D, E, EM, EP$	= coefficient matrices
G	= right-hand-side vector
g	= jacobian of transformation
H	= total enthalpy
L	= characteristic length (throat height)
M	= Mach number
P	= pressure
Pr	= Prandtl number
r	= radial location
Rc	= centerbody radius at throat
Rd	= cowl radius at throat
Re	= Reynolds number
t	= time
U, V	= contravarient velocities
X, Y	= Cartesian coordinates
γ	= ratio of specific heats
μ	= viscosity
ρ	= density
τ	= nondimensionalized time ($\tau = tL/U_\infty$)
$\delta\phi$	= solution vector
ξ, η	= transformed coordinates
$\Delta\xi$	= grid spacing in ξ direction
ω	= flux-splitting parameter

Subscripts

i, j	= indices in ξ, η directions
∞	= freestream conditions
ξ, η	= derivatives

I. Introduction

ACCURATE estimates of the flight characteristics and performance of aircraft propulsion systems require, in part, a systematic and comprehensive evaluation of the flow behavior in the engine diffuser inlet. At supersonic flight Mach numbers, this involves careful analysis of the nature of the shock interactions and of the location of the terminal shock wave. For a given diffuser design, at specific flight conditions, the shock can move ahead of the cowling so that inlet unstart occurs. This causes a sharp reduction in mass flow and pressure recovery and an associated large increase in drag. The shock can be swallowed by increasing the Mach number, by increasing the throat area, or by decreasing the back pressure; engine restart occurs and improved inlet performance is recovered.

The transient unstart/restart of typical aircraft engine inlets is investigated numerically, herein, with a flux-split procedure that can be applied to either the Euler or reduced Navier-Stokes (RNS) equations. The present authors have previously investigated inviscid and viscous flow fields in engine inlets. Unstart and restart were initiated by varying the back pressure and by providing bleed on the surface. References 1–4 provide details of the numerical shock capturing and viscous flow analysis and include a variety of results. In the present study unstart and restart are investigated by varying the throat area. Inviscid and viscous turbulent flow fields are efficiently computed. A two-dimensional/axisymmetric flow solver for inlet flowfield studies has been developed. The governing equations are written in general nonorthogonal curvilinear coordinates and are discretized using a form of flux vector splitting.[5] This procedure was developed previously by Rubin and Reddy[6] and Khosla and Lai.[7] The methodology remains unchanged for viscous or inviscid, incompressible, subsonic, transonic, or supersonic flows (see Refs. 8–11), and has been extended for three-dimensional,[12] as well as unsteady[1–4,13,14] flow computations. Moreover, there is no requirement for explicitly added artificial viscosity, so that numerical diffusion is solely associated with the accuracy of the discretization.[15]

For unsteady flow analysis, in order to capture the transient behavior efficiently, a more robust and time-consistent procedure has been developed. A direct sparse matrix solver[16,17] has been appropriately modified for a coupled system of equations and is applied herein. The choice of the direct solver is dictated by considerations of stability, robustness, accuracy, and time consistency. For steady computations, the solution technique permits large time increments and has strong convergence properties; whereas, for transient flows, time consistency is maintained in an efficient manner. For strong interaction flows, implicit, time-consistent procedures based on approximate factorization, e.g., ADI, typically do not have strong convergence properties and may require added transient or steady-state artificial viscosity.[18] The sparse matrix direct solver, considered herein, retains the simplicity and robustness of the time-marching procedure, and, as in the steady-state global relaxation formulation, explicitly added artificial viscosity is not required. Moreover, for time-dependent computations, the time-step limitation for the direct solver is much less severe than that for other time-marching procedures. To enhance the efficiency of the procedure further, a

Presented as Paper 90-2130 at the AIAA/SAE/ASME/ASEE 26th Joint Propulsion Conference, Orlando, FL, July 16–18, 1990; received Oct. 15, 1990; revision received July 3, 1991; accepted for publication July 24, 1991.

*Research Assistant, Department of Aerospace Engineering and Engineering Mechanics. Student Member AIAA.

†Professor, Department of Aerospace Engineering and Engineering Mechanics. Member AIAA.

‡Professor, Department of Aerospace Engineering and Engineering Mechanics. Associate Fellow AIAA.

domain decomposition strategy is employed. The direct solver is applied in strong interaction regions and a multisweep or global pressure relaxation procedure is applied in predominantly supersonic weak interaction regions.

Since the inlet flow at large Reynolds number is inherently turbulent, an algebraic, two-layer eddy viscosity (Baldwin-Lomax) model[19-21] is considered for turbulent flow closure. Section II presents the governing equations. The boundary conditions and discretization are described in Secs. III and IV, respectively. Section V deals with the solution procedure; the results are discussed in Sec. VI.

II. Governing Equations

The RNS equations are obtained from the full NS equations by neglecting the viscous diffusion terms in an appropriate streamwise direction, as well as all viscous diffusion terms in the surface momentum and energy balances. The conservation form of the RNS equations are written in general nonorthogonal curvilinear coordinates (ξ, η), so that an arbitrary grid generation technique can be applied.

Continuity equation:

$$(\rho gr)_\tau + (\rho grU)_\xi + (\rho grV)_\eta = 0 \tag{1a}$$

X momentum equation:

$$\begin{aligned}&[\rho gr(UX_\xi + VX_\eta)]_\tau + (\rho grU^2X_\xi)_\xi + (\rho grUVX_\eta)_\xi \\ &+ (\rho grUVX_\xi)_\eta + (\rho grV^2X_\eta)_\eta + r(PY_\eta)_\xi \\ &- r(PY_\xi)_\eta - \{\{\mu rX_\xi[U(X_\xi X_\xi - Y_\xi Y_\xi) \\ &+ V(X_\eta X_\xi - Y_\xi Y_\eta)]_\eta/g\}_\eta - \{\{2\mu rY_\xi[2(UX_\xi Y_\xi \\ &+ VX_\eta T_\xi)_\eta + (VrY_\eta X_\xi \\ &+ UrY_\xi X_\xi)_\eta/r]/(3g)\}_\eta\}/(Re_\infty) = 0\end{aligned} \tag{1b}$$

Y momentum equation:

$$\begin{aligned}&[\rho gr(VY_\eta + UY_\xi)]_\tau + (\rho grU^2Y_\xi)_\xi + (\rho grUVY_\eta)_\xi \\ &+ (\rho grUVY_\xi)_\eta + (\rho grV^2Y_\eta)_\eta - r(PX_\eta)_\xi \\ &+ r(PX_\xi)_\eta - \{\{\mu rY_\xi[U(Y_\xi Y_\xi - X_\xi X_\xi) \\ &+ V(Y_\eta Y_\xi - X_\xi X_\eta)]_\eta/g\}_\eta - r\{2\mu X_\xi[3(UY_\xi X_\xi \\ &+ VY_\eta X_\xi)_\eta - (VrX_\xi Y_\eta + UrX_\xi Y_\xi)_\eta/r \\ &+ (UY_\xi X_\xi + VX_\eta Y_\xi)_\eta]/(3g)\}_\eta/(Re_\infty) \\ &- \{r\mu Y_\xi[U(Y_\xi Y_\xi - X_\xi X_\xi) + V(Y_\xi Y_\eta \\ &- X_\eta X_\xi)]_\eta/(g)\}_\eta/(Re_\infty) = 0\end{aligned} \tag{1c}$$

Energy equation:

$$\begin{aligned}&(\rho grH)_\tau + (\rho grHU)_\xi + (\rho grHV)_\eta \\ &= \{r(\gamma - 1)M_\infty^2/[1 + 0.5(\gamma - 1)M_\infty^2]\}(Pg)_\tau \\ &- \{[\mu rY_\xi(HY_\xi)_\eta/g]_\eta + [\mu rX_\xi(HX_\xi)_\eta/g]_\eta\}/(Re_\infty Pr)\end{aligned} \tag{1d}$$

Equation of state:

$$\begin{aligned}&P + (\gamma - 1)\rho V^2/(2\gamma) \\ &= (\gamma - 1)[1/((\gamma - 1)M_\infty^2)) + 0.5](\rho H/\gamma)\end{aligned} \tag{1e}$$

Two-dimensional flow equations are recovered by setting r to one in the above equations (1a–1e). For viscous flow computations, the X and Y momentum balance equations are appropriately combined to obtain the momentum balance in the ξ and η directions. Viscous terms are retained only in the ξ momentum equation; all viscous terms in the η momentum and energy equations are neglected.

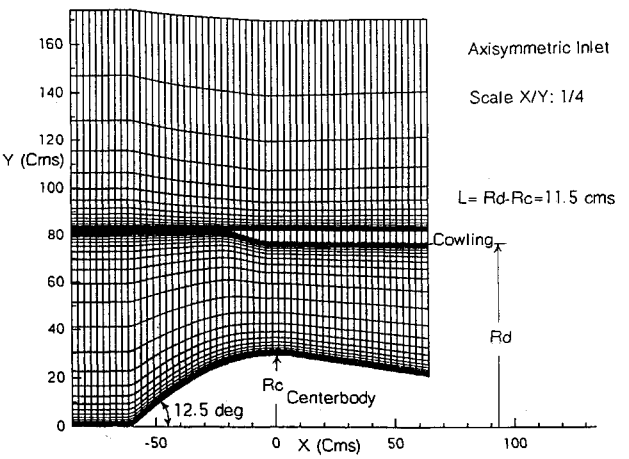

Fig. 1a Axisymmetric inlet I.

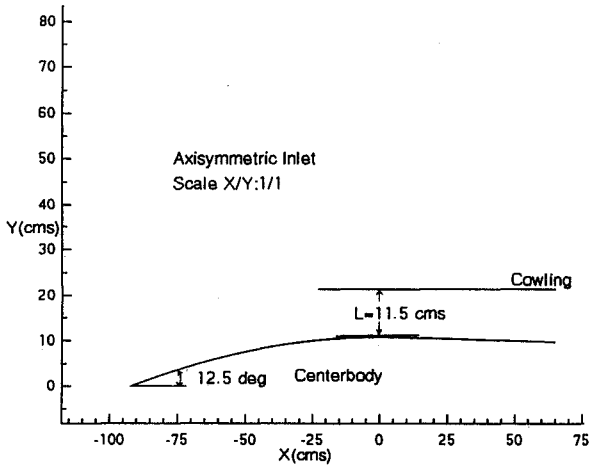

Fig. 1b Axisymmetric inlet II.

In Eqs. (1a–1e) all distances have been normalized with respect to the inlet throat height (Figs. 1a and 1b); the velocities, density, temperature, total enthalpy, and viscosity are nondimensionalized with respect to the corresponding freestream values. The pressure is nondimensionalized with respect to twice the freestream dynamic pressure.

For the turbulent flow computations the Baldwin-Lomax (B-L) model[19,20] is applied herein. The required B-L length scales, associated with each wall layer, are independently determined. This is accomplished by separate scans. The final eddy viscosity is obtained with a composite of these two values. It is well known[21] that the B-L turbulence model is not completely adequate for highly curved geometries or large regions of recirculation. However, for the present application, other available closures do not appear to provide any definitive advantage over algebraic mixing length models, and, in addition, higher order closures incur increased computational cost. While improved turbulence closure models are certainly required in order to assess quantitative flow behavior more accurately, based on the current computations and earlier comparisons[4] with experiments, the B-L model appears to provide reasonable qualitative agreement with the expected transient flow behavior for shock propogation and shock–boundary-layer interaction. This is the primary goal of this study. The present procedure can also be adapted for direct numerical simulation for flows of this type, and this might aid in the development of more accurate closure models. How-

ever, this will require much finer grid resolution and should be considered independently. This study represents a starting point for inlet simulation. In this initial study the B-L model provides useful qualitative assessment of the effects of inlet transients and changes in boundary conditions.

III. Initial and Boundary Conditions

Uniform flow values are generally assumed as initial conditions for the inviscid computations. For viscous flow computations, the inviscid flow values are prescribed as the initial values. Boundary conditions are such that, at the inflow U, V, ρ, P, and H are all prescribed. At the outflow, for boundaries outside of the inlet and far from regions of reversed flow, the negative eigenvalue fluxes are neglected. For internal flow boundaries, the back pressure is specified. This is consistent with the operational or experimental conditions of the inlet. Far from the surface of the cowling, uniform flow conditions are imposed. At the surface, for inviscid flow calculations, zero normal velocity or injection is specified. Since grid speeds are not included in the governing equations, moving walls are treated in a quasisteady manner. For viscous flow computations, additional no-slip and adiabatic wall temperature conditions have been prescribed for most computations. However, cold wall temperature conditions have also been considered in some calculations. Computations are performed for Prandtl number of one. A wall pressure condition is not required. The surface pressure is computed as part of the solution. For external outer boundaries, the freestream pressure is specified. More details on boundary condition applications to internal flows are available in Refs. 1–4 and 22.

IV. Discretization

The RNS equations are discretized based on a pressure flux-split technique. The differencing has been described in previous Refs. 1–5 and is only briefly reviewed here. All convective or ξ derivatives are upwind or flux vector differenced. The η derivatives in the continuity and η momentum equations are two-point central or trapezoidal differenced, whereas, the η derivatives in the ξ momentum and energy equations are three-point central differenced. The three-point η differencing in the ξ momentum and energy equations works quite well for normal shocks, but leads to oscillations ahead of strong oblique shocks. These oscillations are eliminated with two-point differencing, similar to that used for the continuity and η momentum equations. For compression regions the ξ momentum equation, written at an appropriate half-point, or averaged over half-points as in the "box scheme," is employed. For expansion regions the three-point central differencing scheme is retained. The details of this analysis, which depend strongly on matrix diagonal dominance considerations, are given in Ref. 1.

The streamwise pressure gradient is flux-split.[5] This splitting is consistent with the flow physics and does not involve any discontinuous switching across shocks or contact discontinuities. The pressure gradient is given by $P_\xi = (\omega_{i-1/2}) \times (P_i - P_{i-1})/\Delta\xi_i + (1. - \omega_{i+1/2})(P_{i+1} - P_i)/\Delta\xi_i$. The parameter ω is computed as follows: For unsteady flows, where a differential form of the energy equation is employed (see Ref. 5), the Cartesian form of ω is $\omega = M_\xi^2$ for $M_\xi < 1$, and $\omega = 1$, for $M_\xi > 1$.

For curvilinear coordinates, the eigenvalue analysis indicates that the parameter ω should be redefined as follows (for details see Ref. 3): $\omega = \min\{U^2 \cdot g^2/a^2(Y_\eta^2 + X_\eta^2), 1\}$, where Y_η, X_η and g are the metric quantities described previously in Sec. 2.

The flux form of the streamwise pressure gradient term, with ω given at the half-point is second-order accurate.[5] This representation captures very sharp normal shocks, e.g., over three grid points. It should be noted that the flux splitting is employed only in the main flow or ξ direction. In the normal and/or secondary flow direction, as described previously, central two- or three-point differencing is applied. This discretization is capable of capturing very strong normal shocks; however, a complete flux-split formulation in both coordinate directions is required when considering very strong oblique shock waves, e.g., hypersonic freestreams. It should be noted that, although the convective streamwise derivatives are approximated using first-order differencing, the accuracy of the overall scheme is somewhere between first- and second-order for RNS solutions. This analysis has previously been discussed in Refs. 6 and 9. In reversed flow regions, the streamwise convection terms in the ξ momentum and energy equation are flux vector or upwind differenced and this requires that the parameter ω be set to zero (see Refs. 2–5, 13, 15). The discretization is first-order implicit in time.

In subsonic attached flow regions, upstream influence is transmitted through the negative eigenvalue flux or forward differenced part of P_ξ. At the leading edge, upstream influences originate from both the upper and lower surfaces of the cowling. This is modeled with the averaged or "box" representation of the ξ momentum equation, written at two half-points. The details of this are discussed in Ref. 3 and will be elaborated on in a future paper.

V. Solution Procedure

The discretized equations are quasilinearized and written in a nine-point star in delta form:

$$A_{ij}\delta\phi_{ij-1} + B_{ij}\delta\phi_{ij} + C_{ij}\delta\phi_{ij+1} + D_{ij}\delta\phi_{i-1j} + E_{ij}\delta\phi_{i+1j} + AM_{ij}\delta\phi_{i-1j-1} + CM_{ij}\delta\phi_{i-1j+1} + EM_{ij}\delta\phi_{i+1j-1} + EP_{ij}\delta\phi_{i+1j+1} = G_{ij} \tag{2}$$

For supersonic regions, where there is no upstream influence, E_{ij}, EM_{ij} and EP_{ij} are zero, and the method reduces to a standard initial value problem. This system can then be easily solved using a marching technique such as line relaxation. For mildly subsonic flowfields, a global pressure relaxation procedure can be applied. For strong interaction flowfields, the convergence rate of such an iterative technique is rather slow. For unsteady flows the time-step limitation is also severe.[17] Moreover, iterative schemes for strongly interacting flows are susceptible to false transients. Most of the difficulties encountered by iterative or approximation factorization techniques can be overcome by the use of a direct solver. In the present study the choice of direct solver is dictated by considerations of matrix sparsity, stability, robustness, and time consistency.

The Yale Sparse Matrix Package (YSMP), developed by Eisenstadt et al.[17] and modified for coupled systems and for the boundary conditions detailed previously, is applied here. This is an efficient solver as it stores only nonzero elements, and reorders the matrix using a minimum degree algorithm to minimize fill-in during the LU decomposition. However, for fine meshes and large numbers of mesh points, the memory requirement for the direct solver can become significant. Although memory associated with present-day computers has constantly been increasing, access is limited. To overcome this limitation, a domain decomposition strategy is employed. The computational domain is appropriately split into subdomains with suitable overlap between adjacent regions. Since we are dealing with flowfields that involve moving shocks, the overlap has to be sufficiently broad to accommodate the shock capturing. Since numerical shocks are spread over three to four grid points, an overlap of five points is specified. For further details see Ref. 2. If the entire flowfield is solved with a direct solver, in conjunction with the domain decomposition strategy, then the overall rate of convergence is marginally affected. However, the efficiency of the procedure is enhanced by selecting a suitable solution technique for each subdomain. The direct solver is applied in regions of strong interaction, e.g., in the vicinity of the shock, while the re-

mainder of the flowfield is evaluated with the more cost-effective global pressure relaxation technique.

VI. Results

The present authors have previously investigated inviscid and viscous laminar/turbulent flow for a simplified two-dimensional inlet (flat-plate diffuser).[1,2] Rather interesting flow physics are highlighted even by this simple geometry. Unstart and restart was investigated by varying the back pressure and also by applying bleed on the surface. Shock–boundary-layer interaction, time-varying shocks, and recirculation regions were efficiently computed. The flow behavior outside and within a more complex axisymmetric inlet with a centerbody was also investigated. Once again, unstart and restart was initiated by varying the back pressure. The results of this analysis are discussed in Ref. 3.

In the present study inviscid and viscous investigations of the transient flow for axisymmetric inlets with a centerbody (Figs. 1a and 1b) are continued. However, unstart and restart of the inlet are a result of varying the throat area. The grid for this geometry is generated using algebraic interpolation; a shearing transformation is applied. Supersonic flow for an axisymmetric inlet with a centerbody, as shown in Fig. 1a, is considered. Turbulent viscous flows for this geometry are investigated for a Reynolds number of 10^6. Computations were performed on grids of 89 × 115 ($\Delta X/L = 0.16$, $\Delta Y_{min}/L = 4 \times 10^{-5}$) and 115 × 150 ($\Delta X/L = 0.1$, $\Delta Y_{min}/L = 1 \times 10^{-5}$) points. Figure 2 depicts the centerbody pressure variation and Fig. 3 depicts the centerbody skin friction variation on the two grids. On the finer grid the shock structure (Fig. 2) is clearly resolved. Since three-point shocks are captured, the shock on the fine grid is spread over a smaller distance and is sharper. Although the overall solution accuracy is changed only slightly from the other coarse-grid calculations not included here, we can conclude that this finer grid provides a solution that will only be minimally affected with further grid refinement. For this thin turbulent boundary layer, the shock–boundary-layer interaction is quite weak and, as a result, the flow is attached everywhere. This differs considerably from the earlier laminar flow calculations, where regions of recirculation are evident.

Unstart and restart of an axisymmetric inlet (Fig. 1b) are investigated herein by varying the throat area. In this study, to simplify the geometry, a cowling surface of zero thickness is considered. Unstart and restart can be accomplished either by moving the centerbody or by changing the throat area. Since grid speeds are not included, it was more appropriate and feasible to consider unstart/restart by changing the throat radius. Once again, as a first step, the inviscid flow solution is obtained. The flow within the inlet undergoes compression through a system of oblique waves. The effect of progressively decreasing the throat radius (area) is depicted in Fig. 4; as the throat radius is reduced, the oblique shock waves become stronger. This is evident by the surface pressure distribution (Fig. 4). For an inlet operating at design conditions (restarted inlet with no terminal shock), the exit pressure is determined by the flight conditions and the area variation. The inviscid solution for the nondimensional throat radius of 0.227 (Fig. 4) is taken as an initial guess, the exit conditions are held fixed. The throat radius is then reduced by 7.4% (from 0.227 to 0.21) instantaneously. Since for the new throat radius the mass flow entering the inlet is now greater than the allowable, the oblique shock system within the inlet coalesces to form a normal shock wave. This occurs in a nondimensional time of 8. The normal shock wave lies ahead of the throat and as the flow evolves in time, the shock increases in strength and moves towards the cowling tip. The flow behind the normal shock wave is subsonic; the flow reaccelerates to sonic velocity at the throat. The captured mass flow is now greater than the allowable value at the throat. As a result, the shock is expelled out of the inlet. A bow shock forms and unstart of the inlet occurs. The excess mass is spilled over the cowling. The time history leading to unstart is depicted in Figs. 5a–5c. The surface pressure variation indicates that during the initial stages, the shock strength rises rapidly. The pressure contours (Figs. 5b and 5c) depict the shock pattern that exists at various time instants during unstart. At a nondimensional time of 32.2, the shock lies at the tip of the cowling, and at a time of 34.44, it

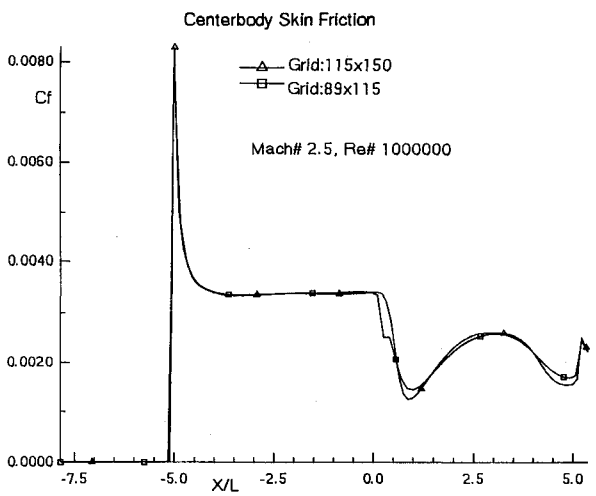

Fig. 3 Skin friction variation.

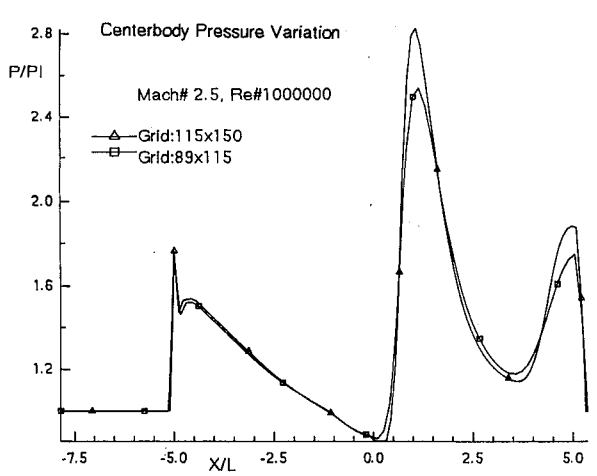

Fig. 2 Pressure variation.

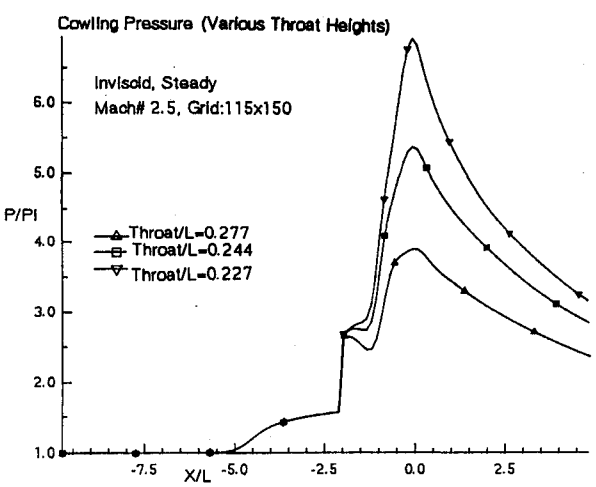

Fig. 4 Pressure variation.

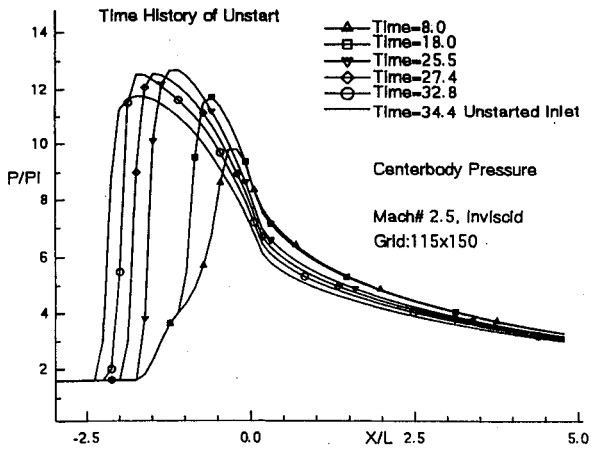

Fig. 5a Time history of unstart.

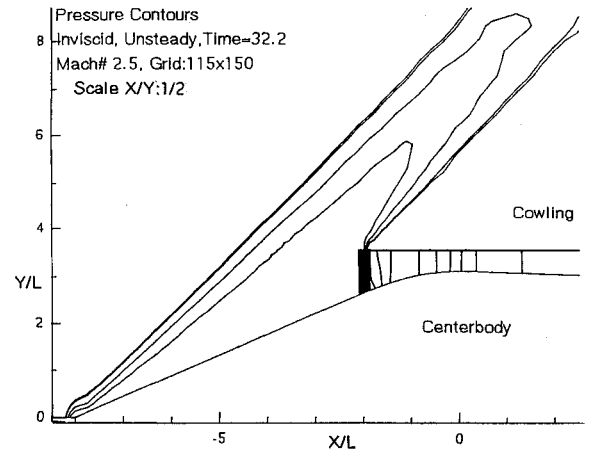

Fig. 5b Pressure contours.

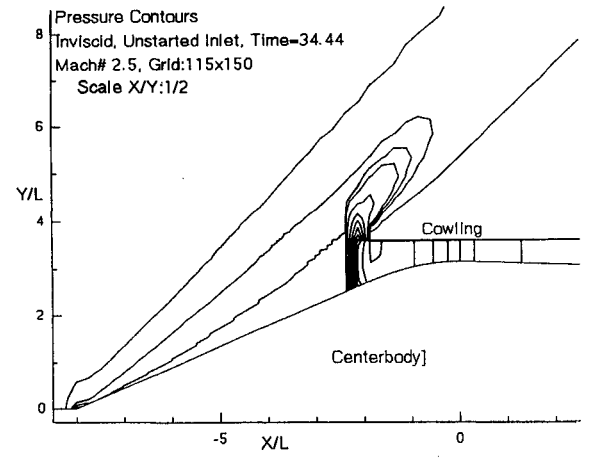

Fig. 5c Pressure contours.

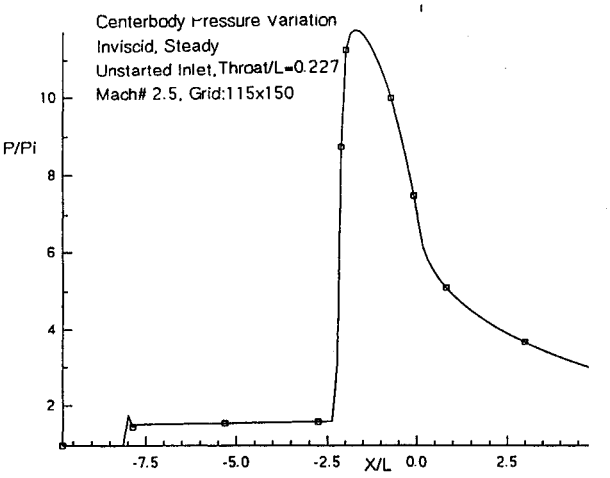

Fig. 6 Centerbody body pressure variation.

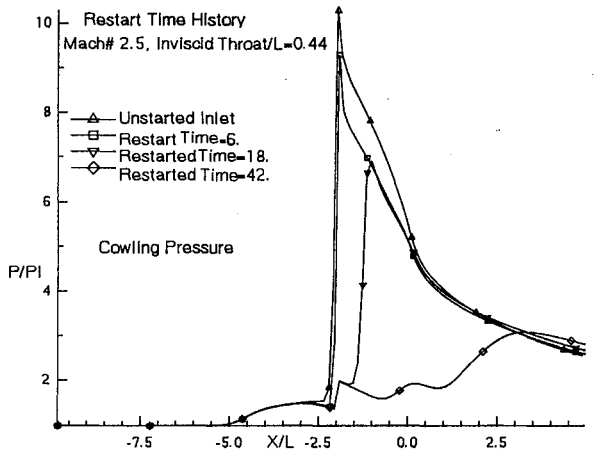

Fig. 7a Time history of restart.

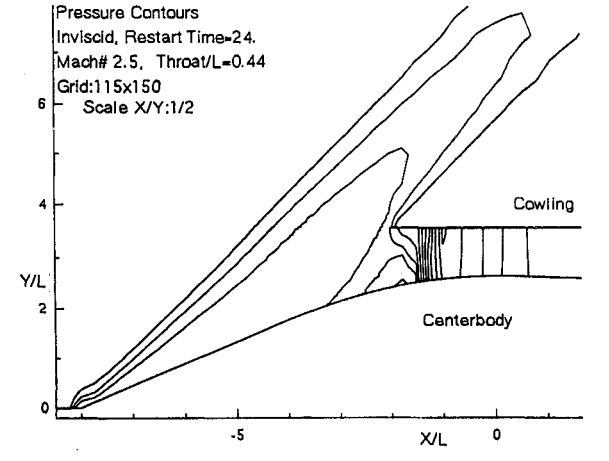

Fig. 7b Pressure contours.

is expelled as a bow shock. This process occurs in a very short time and has been efficiently captured herein.

Inlet restart was investigated by increasing the throat radius. The throat radius was increased to its original value (radius/L = 0.227); restart was not observed. In fact the flow remained in a steady state with a bow shock at a finite distance from the cowling tip (Fig. 6). A further increase in throat radius by 50% failed to restart the inlet. However, when the throat was increased to twice its original radius (radius/L = 0.44), the inlet was restarted. Figures 7a and 7b depict the time history of restart, up to and including the swallowed shock state. The strength of the normal shock wave decreases as it moves towards the throat. In the final state the normal shock wave vanishes and the inlet returns to its original state of a system of oblique shock waves. These solutions are initial condition dependent. For a given throat radius, the inlet can operate in the design condition with no mass spillage or in the off-design unstart condition. From the above results we infer that a slight reduction in the throat will unstart the inlet; however, restart of the inlet requires considerably larger changes in throat radius. This effect will require a further study.

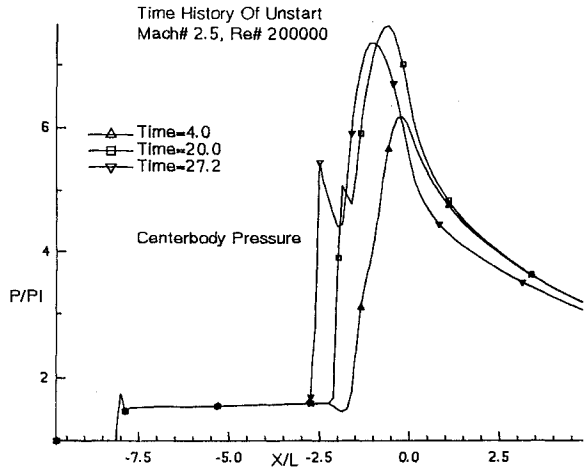

Fig. 8 Time history of unstart.

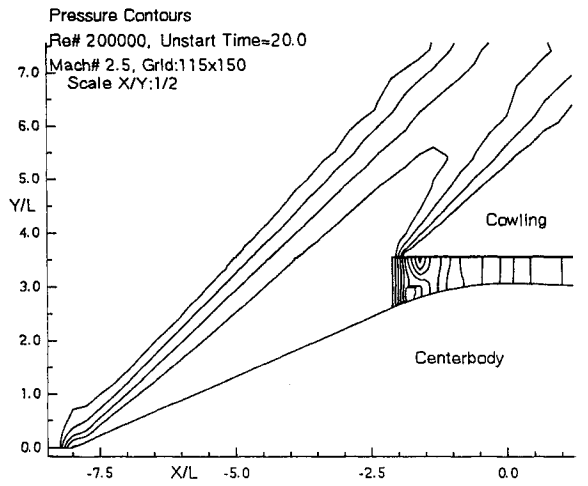

Fig. 9a Pressure contours.

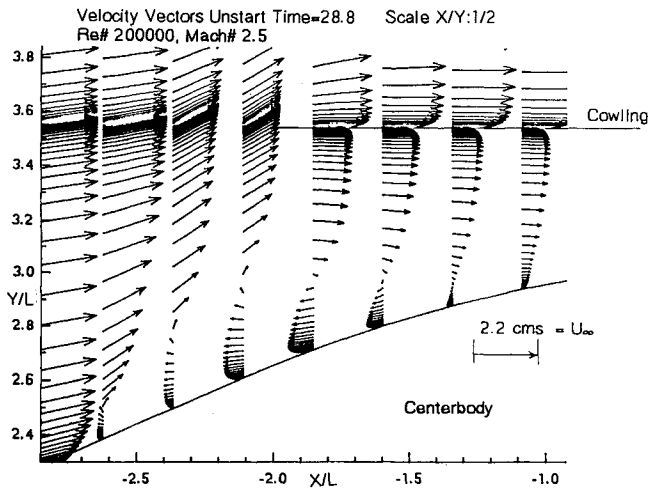

Fig. 9b Velocity vectors.

Several viscous flow computations have also been considered. Turbulent flow with $Re_\infty = 2 \times 10^5$ for the geometry of throat radius/$L = 0.227$ is computed. Although the inviscid solutions indicate that the inlet is operating in the design case with no spillage, the viscous computations indicate that inlet unstart has occurred. This result indicates that boundary-layer interaction plays a significant role in determining the inlet flow behavior. Turbulent flow solutions depicting inlet unstart are shown in Figs. 8 and 9. All computations have been performed on the Cray Y-MP/8. For the above grid with three subdomains, the memory required by the Y-MP/8 is a little under 4 megawords. The time required per iteration is 48 s, i.e., about 192 s per time step.

The geometry considered herein represents a typical inlet configuration and is therefore a reasonable starting point for the simulation of transient inlet behavior. Neither other computational nor experimental results are available for comparison purposes. However, qualitative agreement with flow visualization studies has been discussed in Ref. 2. Therefore, the only assessment of accuracy is through grid refinement studies. These have previously been discussed in Ref. 2 and to some extent herein. The code has been previously validated for other geometries by comparison with other known solutions.[1]

VII. Summary

An RNS flux-split procedure has been applied to investigate unstart/restart of aircraft engine inlets. Axisymmetric inlets with a centerbody were considered. A sparse matrix direct solver combined with a domain decomposition strategy has been used to compute the transient flow field efficiently.

Unstart and/or restart of the inlet were initiated by changing the throat radius. A slight reduction in the throat radius can unstart the inlet; however, restart of the inlet requires considerably larger changes in the throat radius. Viscous flow computations not only indicate that boundary-layer interaction plays a significant role in determining the inlet flow behavior, but also depict the complex flow pattern that exists during unstart. The applicability of the RNS flux-split procedure for unsteady flows involving moving shocks and time-varying recirculation regions has been demonstrated.

Acknowledgments

The work has been supported in part by the NASA Lewis Research Center (T. Benson, Technical Monitor) under Grant NAG 3-1178 and in part by the AFOSR (L. Sakell, Technical Monitor) under Grant 90-0096. The computations have been performed on the Cray Y-MP at the Ohio Supercomputer Center.

References

[1]Pordal, H. S., Khosla, P. K., and Rubin, S. G., "Flux-Split Solution Procedure for the Euler Equations," *International Conference on Computational Techniques and Applications*, Brisbane, Australia, 1989, pp. 437–485.

[2]Pordal, H. S., Khosla, P. K., and Rubin, S. G., "A Flux-Split Solution Procedure for Unsteady Flow Calculations," *International Symposium on Nonsteady Fluid Dynamics*, Toronto, Canada, 1990. pp. 167–165.

[3]Pordal, H. S., Khosla, P. K., and Rubin, S. G., "A Flux-Split Solution Procedure for Unsteady Inlet Flows," AIAA 28th Aerospace Sciences Meeting, AIAA Paper 90-0585, Reno, NV, 1990.

[4]Pordal, H. S., Khosla, P. K., and Rubin, S. G., "A Pressure Flux-Split Technique for Computation of Inlet Flow Behavior," *CFD Symposium on Aeropropulsion*, NASA-Lewis, Cleveland, OH, April 1990, pp. 6.1–6.13.

[5]Rubin, S. G., "Reduced Navier-Stokes/Euler Pressure Relaxation and Flux Vector Splitting," *Computers and Fluids*, Vol. 16, No. 4, 1988, pp. 285–290.

[6]Rubin, S. G., and Reddy, D. R., "Analysis of Global Pressure Relaxation for Flows with Strong Interaction and Separation," *Computers and Fluids*, Vol. 11, No. 4, 1986, pp. 281–306.

[7]Khosla, P. K., and Lai, H. T., "Global PNS Solutions for Subsonic Strong Interaction Flow over a Cone-Cylinder Boat-Tail Configuration," *Computers and Fluids*, Vol. 11, No. 4, 1983, pp. 325–339.

[8]Rubin, S. G., "A Review of Marching Procedures for PNS Equations," *Proceedings of a Symposium on Numerical and Physical Aspects of Aerodynamic Flows*, Springer-Verlag, New York, 1982, pp. 171–186.

[9]Rubin, S. G., and Reddy, D. R., "Global PNS Solution for Lam-

inar and Turbulent Flows," 6th Computational Fluid Dynamics Conference, AIAA Paper 83-1911, Danvers, MA, 1983.

[10]Khosla, P. K., and Lai, H. T., "Global Relaxation Procedure for Compressible Solutions of the Steady-State Euler Equations," *Computers and Fluids*, Vol. 15, No. 2, 1987, pp. 215–218.

[11]Ramakrishnan, S. V., and Rubin, S. G., "Global Pressure Relaxation for Steady, Compressible, Laminar, Two Dimensional Flows with Full Pressure Coupling and Shock Waves," Rept. AFL 84-100, Univ. of Cincinnati, Cincinnati, OH, 1984.

[12]Himansu, A., Khosla, P. K., and Rubin, S. G., "Three Dimensional Recirculating Flows," AIAA 27th Aerospace Sciences Meeting, AIAA Paper 89-0552, Reno, NV, 1989.

[13]Ramakrishnan, S. V., and Rubin, S. G., "Numerical Solution of Unsteady Compressible Reduced Navier-Stokes Equations," AIAA 24th Aerospace Sciences Meeting, AIAA Paper 86-0205, Reno, NV, 1986.

[14]Ramakrishnan, S. V., and Rubin, S. G., "Time Consistent Pressure Relaxation Procedure for Compressible Reduced Navier-Stokes Equations," *AIAA Journal*, Vol. 25, No. 7, 1987, pp. 905–913.

[15]Rubin, S. G., and Himansu, A., "Convergence Properties of High Reynolds Number Separated Flow," *International Journal for Numerical Methods in Fluids*, Vol. 9, No. 11, 1989, pp. 1395–1411.

[16]Bender, E. E., "The Use of Direct Sparse Matrix Solver and Newton Iteration for the Numerical Solution of Fluid Flow," Ph.D. Thesis, Univ. of Cincinnati, Cincinnati, OH, 1988.

[17]Eisenstadt, S. G., Gursky, M. C., Schultz, M. H., and Sherman, A. H., "Yale Sparse Matrix Package II. The Non-Symmetric Codes," Yale Univ. Dept. of Computer Science, Rept. 114, New Haven, CT, 1977.

[18]Khosla, P. K., and Rubin, S. G., "Consistent Strongly Implicit Iterative Procedure for Two-Dimensional Unsteady and Three-Dimensional Space-Marching Flow Calculations," *Computers and Fluids*, Vol. 15, No. 4, 1987, pp. 361–377.

[19]Baldwin, B. S., and Lomax, H., "Thin Layer Approximation and Algebraic Model for Separated Turbulent Flows," AIAA 16th Aerospace Sciences Meeting, AIAA Paper 78-257, Huntsville, AL, 1978.

[20]Visbal, M., and Knight, D., "The Baldin-Lomax Turbulence Model for Two-Dimensional Shock-Wave Boundary-Layer Interactions," *AIAA Journal*, Vol. 22, No. 7, 1984, pp. 921–927.

[21]Nallasamy, M., "Turbulent Models and Their Applications to the Prediction of Internal Flows," *Computers and Fluids*, Vol. 15, No. 15, 1987, pp. 151–194.

[22]Reddy, D. R., and Rubin, S. G., "Consistent Boundary Condition for Reduced Navier-Stokes Scheme Applied to Three-Dimensional Internal Viscous Flows," AIAA 26th Aerospace Sciences Meeting, AIAA Paper 88-0714, Reno, NV, 1988.